Technology

Developmental Cell

# Transcriptional Heterogeneity of Beta Cells in the Intact Pancreas

## Graphical Abstract

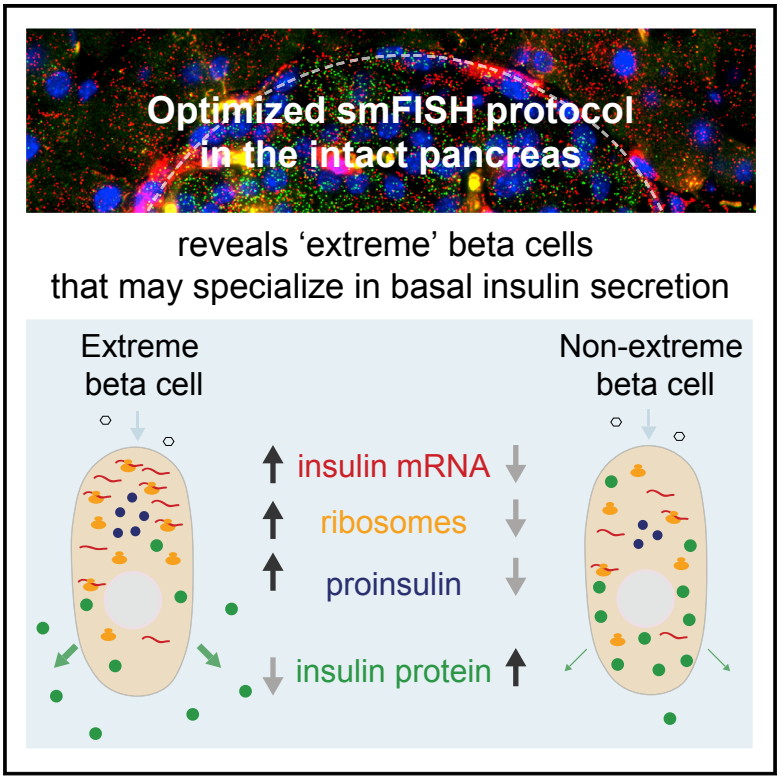


## Highlights

- Islets contain a minority of "extreme" beta cells with elevated insulin mRNA levels
- Elevated proinsulin yet lower insulin protein suggests these are basal secretors
- Extreme cells exhibit discordant apical-basal mRNA and protein localization
- The proportion of extreme cells increases in insulin-resistant animals

## Authors

Lydia Farack, Matan Golan, Adi Egozi, ..., Lior Roitman, Valery Krizhanovsky, Shalev Itzkovitz

## Correspondence

shalev.itzkovitz@weizmann.ac.il

## In Brief

Using an optimized protocol for single-molecule transcript imaging of the intact pancreas, Farack, Golan, et al. reveal that a small subset of beta cells harbors elevated levels of ribosomes and insulin mRNA, suggesting a sub-specialization in basal insulin secretion.

Farack et al., 2019, Developmental Cell *48*, 1–11
January 7, 2019 
https://doi.org/10.1016/j.devcel.2018.11.001

CellPress

Please cite this article in press as: Farack et al., Transcriptional Heterogeneity of Beta Cells in the Intact Pancreas, Developmental Cell (2018), https://doi.org/10.1016/j.devcel.2018.11.001

Developmental Cell
Technology

# Transcriptional Heterogeneity of Beta Cells in the Intact Pancreas

Lydia Farack,[1,3] Matan Golan,[1,3] Adi Egozi,[1] Nili Dezorella,[2] Keren Bahar Halpern,[1] Shani Ben-Moshe,[1] Immacolata Garzilli,[1] Beáta Tóth,[1] Lior Roitman,[1] Valery Krizhanovsky,[1] and Shalev Itzkovitz[1,4,*]
[1]Department of Molecular Cell Biology, Weizmann Institute of Science, Rehovot 7610001, Israel
[2]Department of Chemical Research Support, Weizmann Institute of Science, Rehovot 7610001, Israel
[3]These authors contributed equally
[4]Lead Contact
*Correspondence: shalev.itzkovitz@weizmann.ac.il
https://doi.org/10.1016/j.devcel.2018.11.001

## SUMMARY

**Pancreatic beta cells have been shown to be heterogeneous at multiple levels. However, spatially interrogating transcriptional heterogeneity in the intact tissue has been challenging. Here, we developed an optimized protocol for single-molecule transcript imaging in the intact pancreas and used it to identify a sub-population of "extreme" beta cells with elevated mRNA levels of insulin and other secretory genes. Extreme beta cells contain higher ribosomal and proinsulin content but lower levels of insulin protein in fasted states, suggesting they may be tuned for basal insulin secretion. They exhibit a distinctive intra-cellular polarization pattern, with elevated mRNA concentrations in an apical ER-enriched compartment, distinct from the localization of nascent and mature proteins. The proportion of extreme cells increases in *db/db* diabetic mice, potentially facilitating the required increase in basal insulin. Our results thus highlight a sub-population of beta cells that may carry distinct functional roles along physiological and pathological timescales.**

## INTRODUCTION

The endocrine cells in the pancreatic islets of Langerhans secrete insulin and glucagon in response to glucose perturbations to maintain glucose homeostasis. The insulin-secreting beta cells exhibit morphological, functional, and molecular variations, suggesting that they may consist of sub-populations with specialized tasks and physiological responses (Gutierrez et al., 2017; Roscioni et al., 2016). Features of beta cell heterogeneity include glucose responsiveness and secretory activity (Dorrell et al., 2016; Kiekens et al., 1992; Salomon and Meda, 1986; Van De Winkel and Pipeleers, 1983), proliferative capacity (Bader et al., 2016; van der Meulen et al., 2017; Singh et al., 2017), and electrical activity (Benninger et al., 2014; Bertram et al., 2000; Johnston et al., 2016). Single-cell RNA sequencing (RNA-seq) studies (Baron et al., 2016; Li et al., 2016; Muraro et al., 2016; Segerstolpe et al., 2016; Wang et al., 2016; Zeng et al., 2017) identified sub-populations of beta cells with distinct molecular signatures, for example, in the expression of genes related to endoplasmic reticulum (ER) and oxidative stress. Studies using quantitative RT-PCR identified heterogeneity in the insulin mRNA content of individual beta cells (Bengtsson et al., 2005). However, transcriptional heterogeneity has not been demonstrated in situ.

Exploring beta cell heterogeneity in the intact pancreas requires sensitive techniques to visualize mRNA in situ. Single-molecule fluorescence in situ hybridization (smFISH) has been applied to visualize individual mRNA molecules in diverse mammalian tissues (Halpern et al., 2017; Lyubimova et al., 2013; Moor et al., 2017) as well as in dispersed beta cells (Bahar Halpern et al., 2015; Klochendler et al., 2016). However, this technique has not been successfully implemented in the pancreas. Here, we have optimized the smFISH protocol to facilitate the detection of individual transcripts in the intact mouse pancreas. Using this method, we identified a sub-population of beta cells with higher content of mRNA for insulin and other secretory genes, higher amounts of proinsulin yet lower levels of insulin protein in a fasted state. These cells carry a distinct pattern of polarized mRNA localization and expand in proportions in diabetic *db/db* mice. Our findings thus highlight fundamental features of beta cell heterogeneity, which may be related to distinct functional specialization.

### Design

smFISH has emerged as a powerful tool to assay molecular signatures of individual cells in intact mammalian tissues (Itzkovitz and van Oudenaarden, 2011). Visualizing transcripts in the pancreas, however, has been infeasible without the use of specialized techniques such as photoswitchable dyes (Cui et al., 2018). We have optimized the standard tissue smFISH protocol (Lyubimova et al., 2013) by substantially increasing the period of mRNA denaturation, which precedes the probe hybridization steps, from 5 min to at least 3 hr. In addition, we increased formamide concentrations in both the denaturating wash buffer and hybridization buffer from 10% to 30% (STAR Methods; Methods S1; Figure 1). These modifications facilitated visualizing mRNA of any gene of interest at single-molecule resolution in intact pancreatic tissues (Figure 1A).

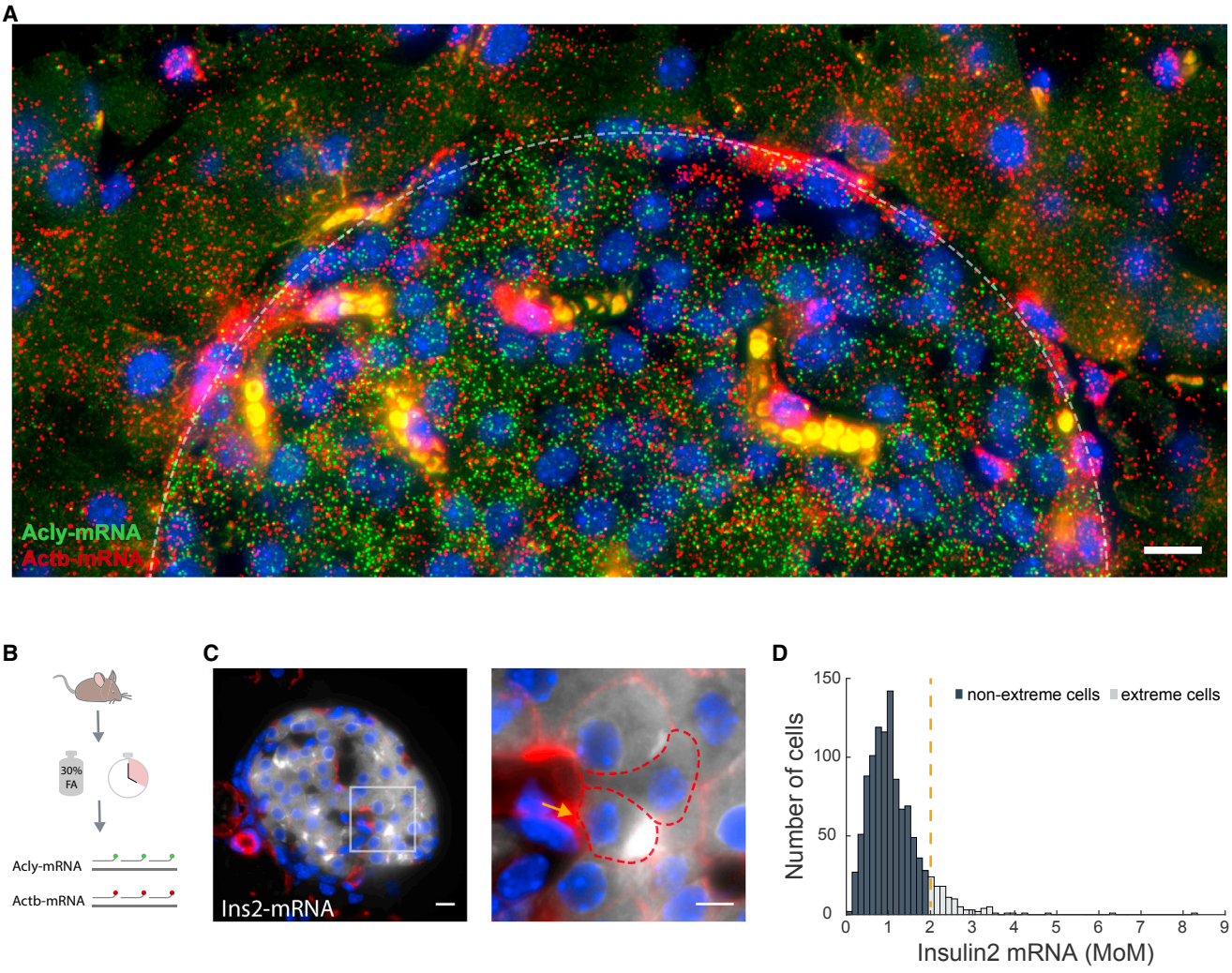


**Figure 1. SmFISH in the Intact Pancreas Reveals Heterogeneity in the mRNA Content of Insulin**

(A) Pancreatic tissue hybridized with smFISH probes for Actb mRNA (red dots) and Acly mRNA (green dots). DAPI-stained nuclei are in blue. Dashed white curve marks the border between an islet and the exocrine tissue. Acly mRNA is highly enriched in endocrine cells of the islet compared to the surrounding exocrine cells, whereas Actb is expressed both within and outside the islet. Yellow is the autofluorescent signal of erythrocytes detected in both channels for Actb and Acly mRNA.

(B) A modified smFISH protocol, using higher formamide concentrations (FA, 30% v/v) and extended mRNA denaturation periods, facilitates single mRNA detection in the intact pancreas (STAR Methods, Methods S1).

(C) An example of an islet stained with smFISH probes for Ins2 mRNA (gray), demonstrating transcriptional heterogeneity among neighboring beta cells. Due to the abundance of Ins2, individual mRNA cannot be discerned; however, cytoplasmic intensity correlates with mRNA content (Little et al., 2013). An extreme beta cell is marked with an arrow. DAPI-stained nuclei are in blue, and phalloidin in red labels the cell membranes.

(D) Distribution of cellular mRNA levels of insulin across beta cells is skewed. Expression is in units of multiple of the median (MoM) cell intensity within the islet. Extreme beta cells are defined as beta cells for which insulin expression exceeded 2-fold the median expression within the containing islet (n = 1,074 cells; 27 islets; 6 mice). All scale bars: 10 μm.

## RESULTS

### Single-Molecule Fluorescence In Situ Hybridization in the Intact Pancreas Reveals Transcriptional Heterogeneity of Insulin

We used our optimized smFISH protocol to measure the cellular mRNA levels of insulin 2 (Ins2). Expression was highly heterogeneous, with mRNA concentrations in cells residing in the same islet often exceeding 2-fold of the median (Figures 1C, 1D, and S1). The distribution of cellular mRNA strongly deviated from normal distribution and was better fitted by a log-normal distribution (Figures 1D and S2). Broad distributions of insulin mRNA levels have been previously measured in dispersed single beta cells (Bengtsson et al., 2005). Our observations demonstrated that this heterogeneity exists within individual islets rather than being generated by distinct insulin expression levels in islets from different pancreatic lobes. We termed the beta cells for which Ins2 expression exceeded 2-fold the median

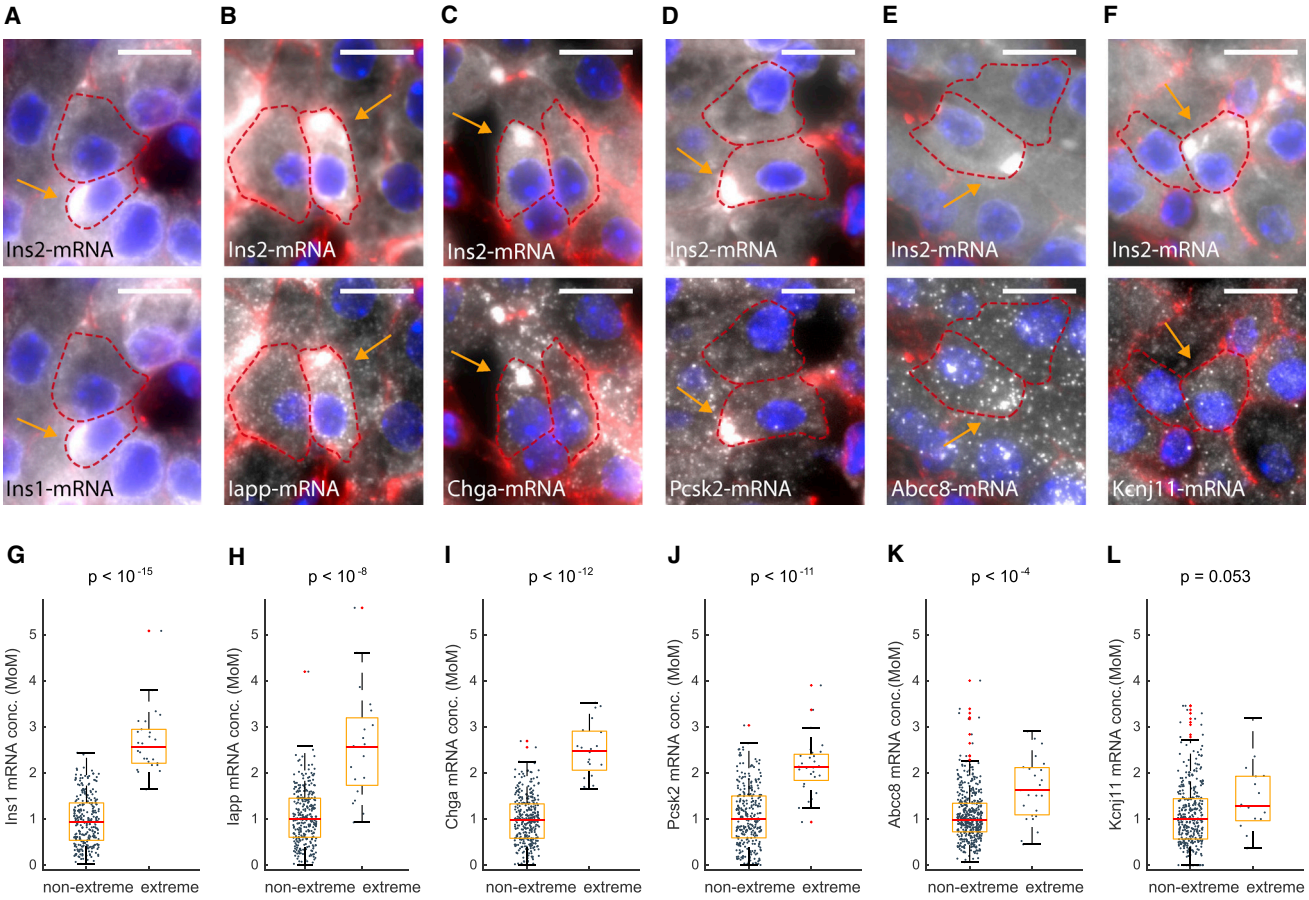


**Figure 2. Extreme Beta Cells Have Significantly Higher Expression Levels of Genes Related to Insulin Processing and Secretion**

(A–L) Islet images demonstrating the correlated mRNA levels of Ins2 and Ins1 (A), Iapp (B), Chga (C), Pcsk2 (D), Abcc8 (E), and Kcnj11 (F). Extreme cells are marked by arrows. DAPI-stained nuclei are in blue, and phalloidin in red indicates cell borders. Scale bars: 10 μm. Quantification of mRNA concentration for Ins1 (G; $p < 10^{-15}$; n = 300 cells), Iapp (H; $p < 10^{-8}$; n = 323 cells), Chga (I; $p < 10^{-12}$; n = 351 cells), Pcsk2 (J; $p < 10^{-11}$; n = 357 cells), Abcc8 (K; $p < 10^{-4}$; 461 cells), and Kcnj11 (L; p = 0.053; n = 374 cells) show higher mRNA levels for extreme cells compared to non-extreme cells. Units of mRNA expression are multiple of median (MoM). Results are based on 7–13 islets from 2–5 mice each. p Values were calculated using the Wilcoxon rank-sum test.

expression within the containing islet "extreme" beta cells. The proportions of extreme beta cells were highly variable among different islets (7% ± 4%; 27 islets; 6 mice). While the spatial distributions of extreme cells were highly heterogeneous among islets, they preferentially appeared in clusters and were more abundant in the center of the islets (Figure S3).

## Extreme Cells Have Higher Expression Levels of Beta Cell Genes Associated with Insulin Secretion

Variability in cellular mRNA levels can stem from intrinsic or extrinsic sources. Intrinsic variability in the mRNA levels of a gene can originate from the stochastic, bursty nature of transcription. Such variability has been demonstrated in bacteria, yeast, and mammalian cells (Eldar and Elowitz, 2010; Raj and van Oudenaarden, 2008). In contrast, extrinsic variability stems from differences between cells in the concentrations of components that are controlling more than one gene, such as activated transcription factors. As such, intrinsic variability results in non-correlated variations, whereas extrinsic variability gives rise to correlated variations in the expression of different genes among different cells (Elowitz et al., 2002).

To discern between extrinsic and intrinsic variability, we performed simultaneous smFISH for pairs of genes that are associated with insulin secretion. In mice, insulin is encoded by the two genes Ins1 and Ins2 (Wentworth et al., 1986). We found a strong correlation between the levels of these two genes (R = 0.98; $p < 10^{-212}$) and significantly higher levels in extreme cells for Ins1 ($p < 10^{-15}$; Figures 2A and 2G) and for the genes encoding islet amyloid polypeptide (Iapp; $p < 10^{-8}$; Figures 2B and 2H) and chromogranin A (Chga; $p < 10^{-12}$; Figures 2C and 2I), both of which are directly associated with insulin secretion. Furthermore, extreme cells had significantly higher levels of Pcsk2, encoding proprotein convertase 2, which is important for proinsulin processing ($p < 10^{-11}$; Figures 2D and 2J).

Insulin secretion in beta cells is regulated by the activity of the ATP-sensitive potassium channel, an octamer composed of the proteins encoded by Abcc8 and Kcnj11. Using smFISH, we found that extreme cells had significantly higher levels of Abcc8 ($p < 10^{-4}$; Figures 2E and 2K), as well as higher, yet not statistically significant, levels of Kcnj11 (p = 0.053; Figures 2F and 2L). Extreme cells also had significantly higher concentrations for additional genes associated with beta cell maturation

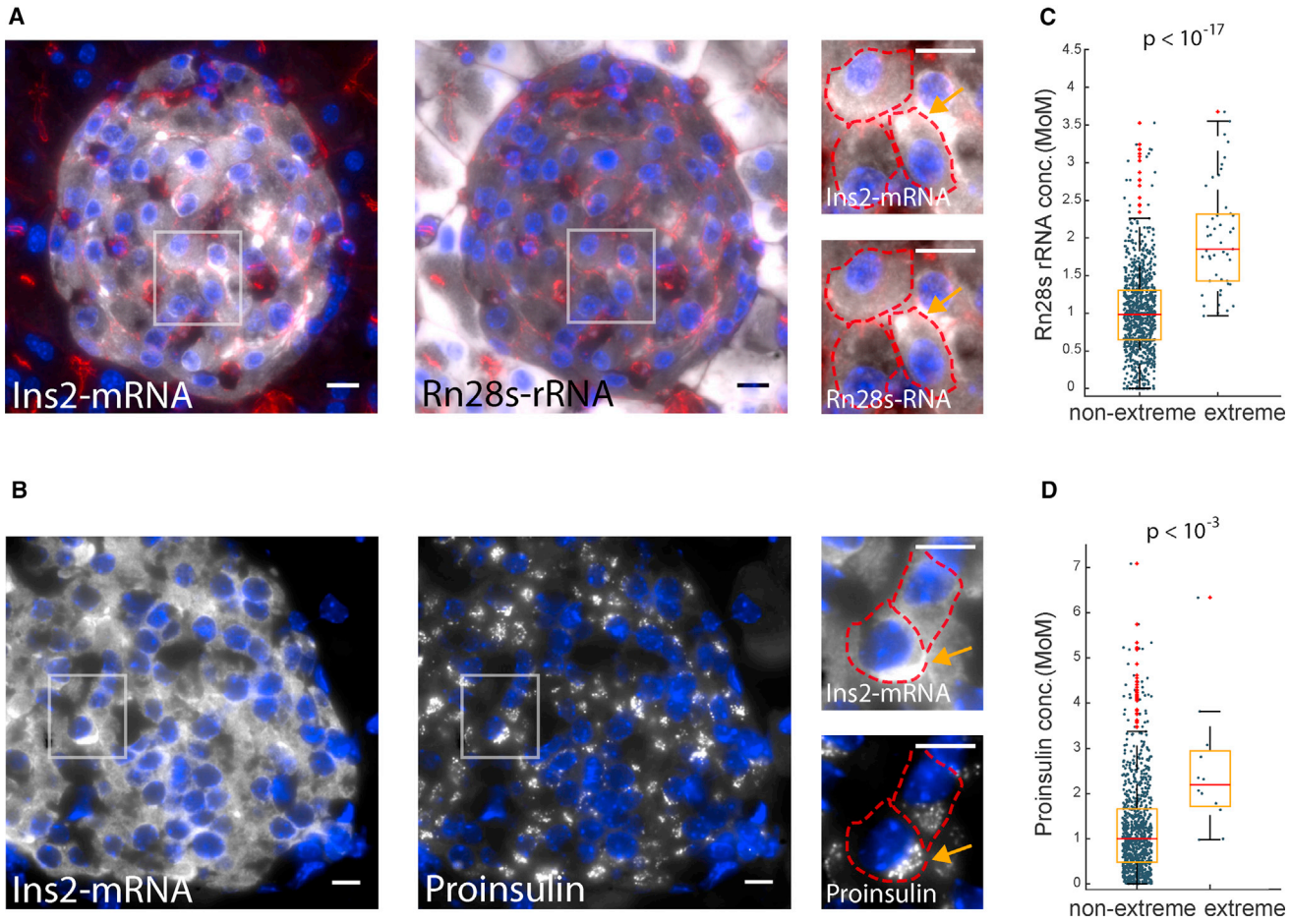


**Figure 3. Extreme Cells Have Higher Levels of Ribosomes and Proinsulin**

(A and B) An islet showing smFISH staining for Ins2 mRNA and (A) Rn28s rRNA, and (B) immunofluorescence for proinsulin. Extreme cells are marked by arrows. DAPI-stained nuclei are in blue. Phalloidin in red labels the cell membranes. All scale bars: 10 μm.

(C) Ribosomal RNA Rn28s concentrations are higher in extreme cells ($p < 10^{-17}$; n = 969 cells; 3 mice).

(D) Proinsulin concentrations are higher in extreme cells ($p < 10^{-3}$; n = 912 cells; 3 mice). p Values were calculated using the Wilcoxon rank-sum test.

and function in rodents—Pdx1, Ucn3, Slc2a2, and Acly (Blum et al., 2012; Chu et al., 2010; Gao et al., 2014; McCulloch et al., 2011; Thorens and Roduit, 1994)—yet not for Rnase4 or Mt1, encoding the zinc buffer metallothionein 1 (Figure S4). Thus, extreme cells carry a distinct molecular signature consisting of elevated levels of both insulin and other genes related to its processing and secretion.

## Extreme Cells Have Higher Levels of Ribosomal Components and Proinsulin but Lower Levels of Mature Insulin Protein

To assess whether extreme cells engage in higher translation of insulin mRNA, we next used smFISH to quantify the levels of ribosomal RNA in the intact pancreas. Extreme cells had significantly higher levels of the ribosomal RNA Rn28s (Figures 3A and 3C; ratio of extreme over non-extreme equals 1.9, $p < 10^{-17}$). To assess whether the increased concentration of ribosomes in extreme cells yields higher translation, we performed simultaneous smFISH measurements for Ins2 and immunofluorescence measurements for the proinsulin protein. Extreme cells had significantly higher abundance of proinsulin (Figures 3B and 3D; ratio of extreme over non-extreme equals 2.2, $p < 10^{-3}$). Thus, extreme cells have higher concentrations of ribosomes and seem to be translating more insulin protein compared to non-extreme beta cells.

The relative abundance of ribosomal components and proinsulin in extreme cells suggested that they may also contain higher levels of mature insulin protein. Surprisingly, using immunofluorescence measurements of the mature insulin proteins, we found that extreme cells had significantly lower protein levels (Figures 4A and 4B; ratio of extreme over non-extreme equals 0.7; $p < 10^{-3}$). The relative depletion of insulin protein was even more striking when examining the protein per mRNA ratios (Figure 4C; ratio of extreme over non-extreme equals 0.2; $p < 10^{-19}$), a factor that is correlated with the ratios of protein degradation and secretion over protein translation (Schwanhäusser et al., 2011). The lower levels of insulin proteins in extreme cells could mean that insulin transcripts are less efficiently translated, that insulin proteins are preferentially degraded, or that they are secreted at a higher rate. The previously reported long protein lifetime of insulin

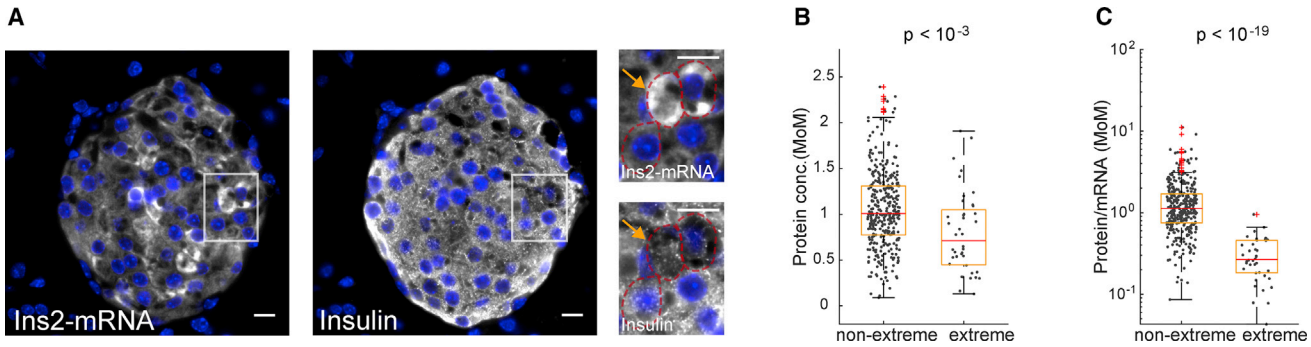


**Figure 4. Extreme Cells Have Lower Levels of Insulin Protein**

(A) An islet image demonstrating anti-correlation between insulin mRNA and protein. Extreme beta cells are marked by an arrow. DAPI-stained nuclei are in blue. Scale bars: 10 μm.

(B and C) (B) Quantification of insulin protein ($p < 10^{-3}$; n = 393 cells; 2 mice) and (C) the ratio of insulin protein per insulin mRNA ($p < 10^{-19}$) show that both are significantly reduced in extreme beta cells. p Values were calculated using the Wilcoxon rank-sum test.

in beta cells (Michael et al., 2006) and our findings of increased ribosome content, as well as Pcsk2 levels in extreme cells, suggest that extreme beta cells may have higher secretion rates compared to non-extreme beta cells, rather than lower translation rates or protein stability. Thus, extreme cells may be tuned toward basal secretion of insulin rather than toward its storage. Notably, however, extreme cells did not exhibit increased accumulation of insulin protein compared to non-extreme cells upon *in vivo* and *ex vivo* application of diazoxide (data not shown), a potassium channel opener that reduces insulin secretion (Gembal et al., 1992).

## Extreme Cells Have an Intra-cellular Apical Polarization of mRNA

Beta cells are highly polarized cells that are spatially arranged in rosette-like structures, with a basal side facing a venous capillary and an apical side surrounded by an arterial capillary (Bonner-Weir, 1988; Gan et al., 2017; Geron et al., 2015; Granot et al., 2009; Weir and Bonner-Weir, 1990). Distinct beta cell faces have been shown to have different properties. The lateral sides are enriched with molecules such as glucose transporters (Orci et al., 1989) and are the sides of more active insulin secretion (Takahashi et al., 2002), whereas the apical sides are the sites of primary cilia projections (Gan et al., 2017).

We found that insulin mRNA in extreme cells was strongly concentrated at the apical sides of the cells (Figures 5A and 5B). Notably, the intra-cellular localization of mRNA did not overlap the baso-lateral localization of mature insulin and the juxtanuclear localization of proinsulin (Figure 5C), an intra-cellular domain previously shown to overlap with the Golgi apparatus (Haataja et al., 2013). Thus, extreme beta cells exhibit an intra-cellular polarization pattern consisting of distinct domains for mRNA and ribosomes and nascent and mature proteins (Figure 5D). The apical polarization of mRNA in extreme cells was not unique to insulin. Rather, the mRNA of other genes such as the neuropeptide Ucn3 and the glucose transporter Slc2a2, as well as the ribosomal RNA28s, was also more concentrated in this apical compartment (Figures 5E and 5F). The enrichment of both mRNA and ribosomal RNA in the apical domain of extreme cells suggests that this is an intra-cellular region with active translation rather than mRNA storage.

To further validate these morphological features of extreme cells, we imaged isolated islets using transmission electron microscopy (TEM). We identified a minority of cells with an extended apical ER (25 out of 224 beta cells; Figures 5G and S5), consistent with our smFISH-based finding on apical enrichment of ribosomal RNA. These cells were relatively depleted of insulin granules, supporting our hypothesis that extreme cells are tuned for both higher translation and higher rates of basal secretion.

## *Db/db* Mice Have Increased Proportions of Extreme Cells

The endocrine pancreas has a remarkable capacity to adapt to elevated blood glucose levels associated with insulin resistance. This adaptation has been shown to entail an increase in the amount of insulin per beta cell, as well as beta cell hypertrophy and hyperplasia (Bock et al., 2003; Dalbøge et al., 2013; Rhodes, 2005). To examine whether insulin resistance affects the balance between extreme and non-extreme beta cells, we performed smFISH measurements of Ins2 on diabetic *db/db* mice and age-matched controls. The islets in *db/db* mice were larger, as previously shown (Dalbøge et al., 2013). Notably, islets in *db/db* mice exhibited a significant increase in the proportion of extreme cells, as seen from the consistent shift in intra-cellular mRNA polarization (Figure 6). As in the controls, insulin protein and mRNA had opposite intra-cellular localization in extreme cells from *db/db* mice (Figure S6). Thus, islet compensation for the systemic insulin resistance in *db/db* mice entails an increase in the relative proportions of extreme cells.

## DISCUSSION

smFISH has been instrumental in revealing molecular identities of cells in a variety of tissues. However, application of this technique in the intact mammalian pancreas has been challenging. Here, we present an optimized protocol for smFISH in the intact mouse pancreas. This technique enables precise transcript measurements of single cells in a range of pancreatic cell types, including the endocrine beta cells, alpha cells and delta cells (Figure S3F), exocrine acinar cells (Figures S7A and S7B), and duct cells of pancreatic intraepithelial neoplasia lesions (Figures

Please cite this article in press as: Farack et al., Transcriptional Heterogeneity of Beta Cells in the Intact Pancreas, Developmental Cell (2018), https://doi.org/10.1016/j.devcel.2018.11.001



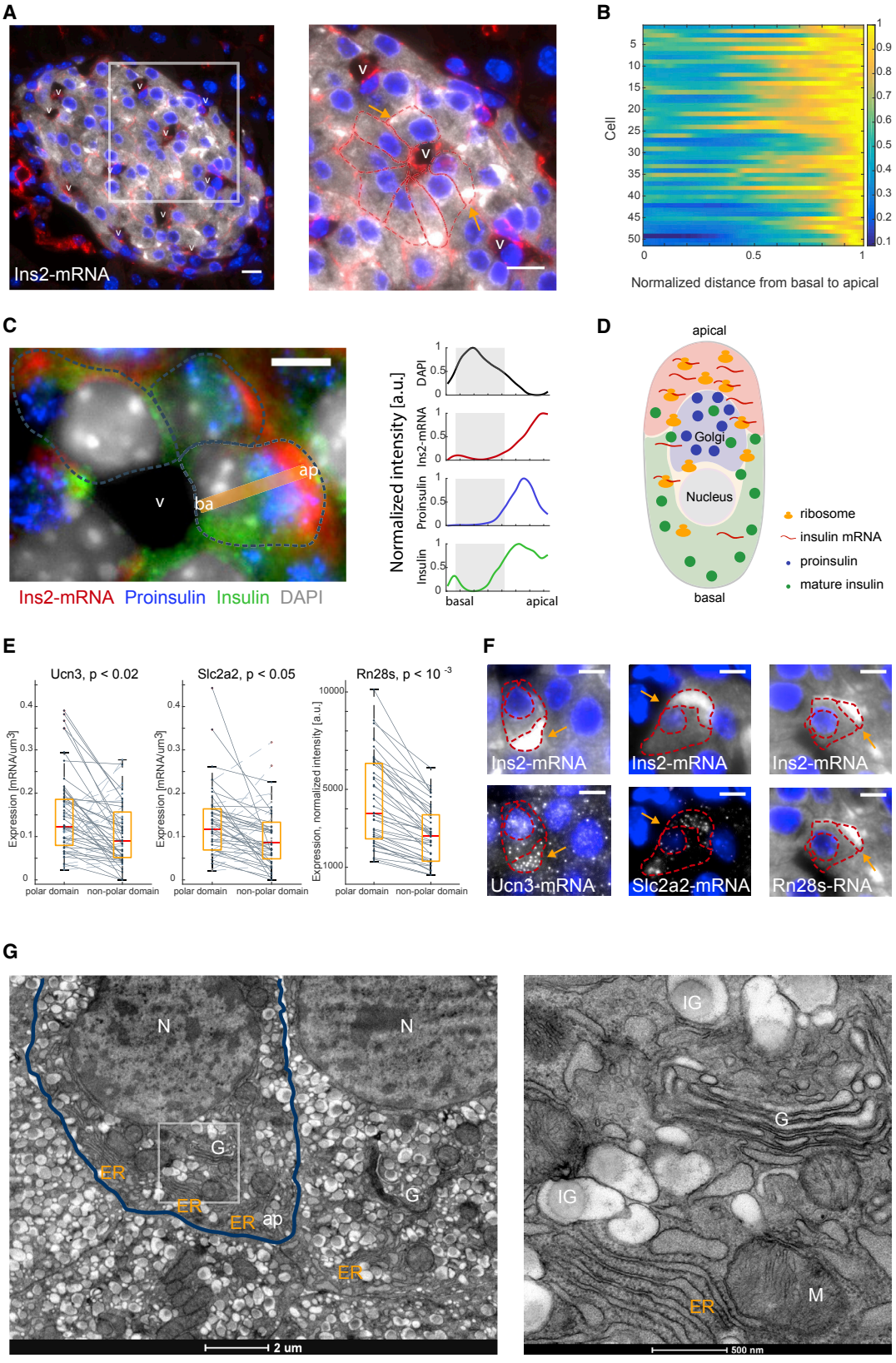


*(legend on next page)*

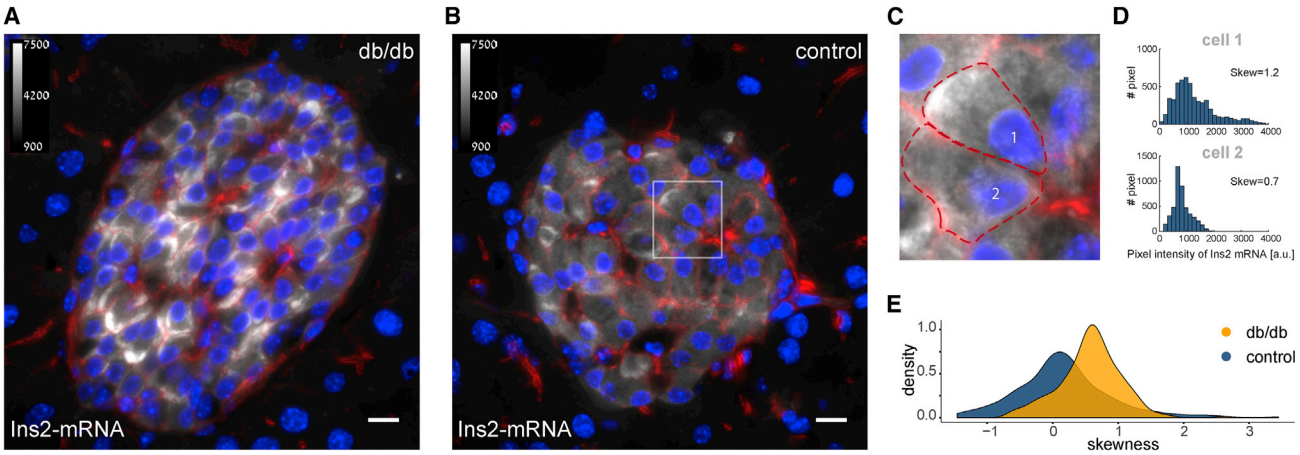


**Figure 6. Proportions of Extreme Beta Cells Are Increased in Diabetic *db/db* Mice Compared to Aged-Matched Control B6 Mice (14- to 15-Week-Old, Male)**

(A and B) An islet of Langerhans from a diabetic *db/db* (A) and control C57BL/6J (B) mouse. Islets were size-matched in this comparison. Ins2 mRNA is in gray, phalloidin in red indicates cell borders, and DAPI-stained nuclei are in blue. The calibration bars indicate the pixel intensity for insulin mRNA. All scale bars: 10 μm.

(C) An example of an extreme beta cell (1) with insulin mRNA polarized on the apical side and a non-extreme beta cell (2) for which insulin mRNA is more uniformly distributed across the cytoplasm.

(D) The distribution of pixel intensities for these two cells shows a stronger positive skew for the extreme (cell 1; skew = 1.2) compared to the non-extreme beta cell (cell 2; skew = 0.7).

(E) Quantification of pixel intensity skewness as a proxy for insulin mRNA polarization for B6 (n = 302 cells; 3 mice) and *db/db* mice (n = 272 cells; 3 mice). The positive shift in the skewness for *db/db* compared to B6 mice ($p < 10^{-24}$; two-sample Kolmogorov-Smirnov test) indicates stronger polarization of insulin mRNA and an enrichment of extreme beta cells in diabetic *db/db* mice.

S7C–S7E). This approach enables exploring pancreatic cell identity while preserving tissue spatial context and can be applied in different metabolic states, in pathologies ranging from diabetes to pancreatic cancer (Ferreira et al., 2017; Hingorani et al., 2003; Yachida et al., 2010) and during organ development (Benitez et al., 2012; Jørgensen et al., 2007; Kim et al., 2015; Sander and German, 1997; Zeng et al., 2017) and regeneration (Aguayo-Mazzucato and Bonner-Weir, 2018; Dor et al., 2004; Nir et al., 2007; Pagliuca and Melton, 2013; Porat et al., 2011). Our technique is also well suited to study dynamics of transcription, mRNA processing, and nuclear mRNA retention, a prominent feature that has been described in *ex vivo* islets (Bahar Halpern et al., 2015) in the intact pancreatic tissue. This technology will also form an important complement to single-cell RNA-seq efforts to map the cell types in the human pancreas (Regev et al., 2017).

Beta cells need to be optimally tuned for two distinct tasks—a constant basal secretion of insulin throughout the day and an abrupt increase in insulin secretion following meals to compensate for the acute elevation in blood glucose levels. These two goals may be mutually exclusive—the capacity to rapidly secrete massive amounts of insulin following a meal requires producing and storing insulin granules over extended times rather than constantly secreting them. Division of labor, where the goals of basal and abrupt secretion are assigned to two distinct pools of beta cells could be a strategy to alleviate this trade-off.

Our study revealed a minority of extreme beta cells that contain higher transcript levels of insulin and other secretory

**Figure 5. Extreme Cells Have an Intra-cellular Apical Polarization of mRNA**

Beta cells are spatially arranged in rosette-like structures surrounding a venous capillary.

(A) An islet image demonstrating apical polarization of insulin mRNA on the distal side of the veous capillary (v). Ins2 mRNA is in gray. Phalloidin in red indicates cell borders, also segmented by dashed red outlines. DAPI-stained nuclei are in blue. Arrows indicate polarized mRNA concentrations on the apical side. Scale bars: 10 μm.

(B) Normalized line profiles from the basal to apical side demonstrate apical insulin mRNA polarization in extreme cells (n = 51 cells). Blue indicates low and yellow high amounts of Ins2 mRNA.

(C) Insulin mRNA (red) is non-overlapping with proinsulin (blue) and mature insulin proteins (green). DAPI-stained nuclei are in gray. Scale bar: 5 μm. A line profile (orange line; line width 10 pixels) from the basal (ba) to apical (ap) side of the cell shows spatially distinct compartments for insulin mRNA and protein. Line plots on the right are quantifications of the line intensity of the four channels. Gray patches show the nuclear area (defined as the region between the half maximum of the DAPI channel).

(D) A cartoon representing the three cellular domains in extreme beta cells—apical (red), juxtanuclear (blue), and baso-lateral (green)—with the distinct localization of ribosomes together with insulin mRNA, proinsulin, and mature insulin, respectively.

(E) Ucn3 and Slc2a2 mRNA, as well as Rn28s rRNA concentrations, are significantly higher in the polarized domain of Ins2 mRNA compared to the remaining non-polar cytoplasmic domain. p Values were calculated using the Wilcoxon rank-sum test.

(F) Extreme cells with increased transcripts of Ucn3, Slc2a2, or Rn28s at the polar apical domain. The polar domain and the non-polar cytoplasmic domain are segmented by dashed red outlines. DAPI-stained nuclei are in blue. Arrows indicate polar domains on the apical side. Scale bars: 5 μm.

(G) Electron micrographs of isolated islets, showing an extreme cell and adjacent non-extreme cells. The extreme cell exhibits apically enriched ER and is relatively depleted of insulin granules. The membrane of the extreme cell is marked by a blue line. Ap, apical side; ER, endoplasmic reticulum; G, Golgi; IG, insulin granule; M, mitochondrion; N, nucleus. The scale bars represent 2 μm and 0.5 μm, respectively.

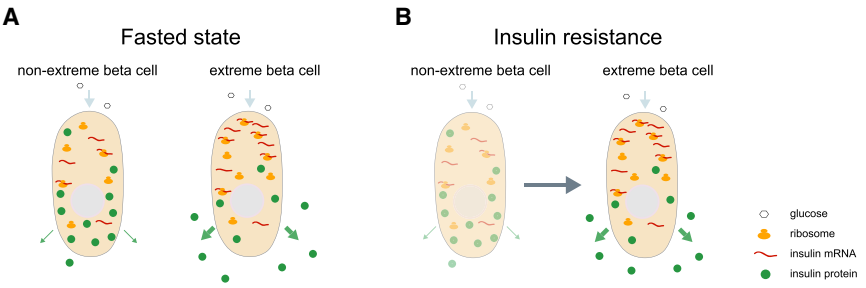


**Figure 7. Model of Extreme and Non-extreme Beta Cells**

(A and B) Extreme beta cells are highly enriched in insulin mRNA and ribosomes but (A) contain lower levels of secretory insulin granules compared to non-extreme beta cells in a fasted state. They might be engaged in basal insulin secretion, whereas non-extreme cells store insulin granules to prepare for a glucose challenge. The non-extreme beta cells can therefore release massive amounts of stored insulin during a glucose challenge, as part of the first phase of insulin response. (B) The ratio of extreme over non-extreme beta cells is increased in insulin-resistant *db/db* mice. The increase of extreme cells might be a result of long-term hyperglycemia and reflects the need for basal insulin secretion at the costs of losing the first phase of insulin response and therefore the ability to respond to the glucose stimulation of a meal.

genes and higher content of ribosomes and proinsulin, but notably lower ratios of insulin protein per mRNA in a fasted state. These properties suggest that extreme cells may be specialized for basal insulin secretion. They may be constantly translating large amounts of insulin proteins, but rather than storing granules intra-cellularly, they preferentially secrete them in fasted states when blood glucose levels are normal (Figure 7A). In contrast, the pool of non-extreme cells might be tuned for accumulating large amounts of insulin during fasted states to facilitate the required burst of secretion after a meal.

The lower levels of insulin protein, together with the higher levels of proinsulin in extreme cells, could alternatively be explained by higher cellular degradation rates of the mature insulin protein, rather than higher rates of secretion. Notably, however, Kiekens et al. (1992) previously identified a sub-population of beta cells with higher levels of proinsulin in a fasted state, a feature we have also observed for extreme cells (Figures 3B and 3D). These cells were both metabolically more active and contained a similar ratio of labeled newly made insulin per proinsulin compared to the other beta cells (Kiekens et al., 1992), arguing against increased protein degradation in extreme cells. To examine the hypothesis that extreme beta cells have a higher insulin secretion rate, we performed diazoxide treatment but did not observe increased accumulation of insulin protein in extreme cells (data not shown). It could be that extreme cells have a higher baseline potassium channel activity compared to non-extreme cells, which could result in an incomplete block of secretion by diazoxide (Gembal et al., 1992). A functional proof of the distinct secretory activity of extreme cells would necessitate approaches to dynamically measure secretion from entire beta cells before fixation for exploration using smFISH. Emerging technologies would enable such future exploration into the dynamic properties of extreme and non-extreme cells in different metabolic states.

The picture of two functionally distinct pools of beta cells could also account for islet malfunction in insulin-resistant states. A hallmark of insulin resistance, which is observed also in *db/db* mice, is the lack of first-phase insulin secretion (Pfeifer et al., 1981; Unger and Orci, 2010). In healthy states, insulin is released in a biphasic manner due to a rapid and sustained increase of glucose following a meal. In the first phase, insulin levels are abruptly elevated over a timescale of 4 to 8 min. The secretory rate then decreases and subsequently gradually increases during the second phase that lasts as long as glucose levels remain high (Henquin et al., 2006). In stark contrast, in diabetic states, glucose-stimulated insulin response lacks the first phase and only ramps up slowly for the second-phase response, leading to elevated blood glucose levels and a slow decline toward the basal glucose level.

Our work suggests that this lack of first-phase insulin secretion could be associated with the change in proportion of extreme and non-extreme cells. In an insulin-resistant state, higher insulin levels are needed in the basal state, to counteract the constantly elevated blood glucose levels. Increased proportions of extreme cells, which are tuned for basal secretion, could be effective in resisting the elevated basal glucose levels. This increase comes at a price, however, of lowering the ability to respond to glucose meals by depleting the non-extreme cells that specialize in the acute glucose response. Thus, the change in proportions of extreme and non-extreme beta cells could be an additional compensatory mechanism to beta cell hyperplasia and hypertrophy aimed at lowering basal blood glucose levels in insulin-resistant states (Figure 7B). Notably, extreme beta cells have higher mRNA levels of Ucn3 and Pdx1 and are thus likely distinct from the recently identified Ucn3-low virgin cells (van der Meulen et al., 2017) and Pdx1-low hub cells (Johnston et al., 2016).

Insulin mRNAs are highly stable with a half-life of 30–80 hr, depending on the metabolic state (Welsh et al., 1985). Thus, reducing the insulin transcripts from the typical levels observed in extreme cells to those in non-extreme cells would require a few days, even in the case of complete cessation of insulin transcription. Thus, the extreme cell state is relatively stable. Future work will examine the dynamics of the shift between non-extreme and extreme cells, the timescales involved, and the potential of the islets to switch back to the normal extreme cell proportions, e.g., when reverting from a high-fat diet.

A notable feature of extreme beta cells is their apical polarization of mRNA. The beta cell cytoplasm of these cells is highly compartmentalized, with mRNA of insulin and other genes, as well as ribosomal RNA, concentrated in an apical ER-enriched compartment, nascent insulin concentrated in a juxtanuclear compartment, and mature insulin in the baso-lateral sides of the cells. Thus, proteins and mRNA in extreme cells seem to be localized in different compartments. Such non-overlapping localization of mRNA and proteins has been recently demonstrated in the intestinal epithelium (Moor et al., 2017). Future work will explore the mechanisms that give rise to this unique global intra-cellular polarization pattern (Buxbaum et al., 2015; Martin and Ephrussi, 2009) and the potential advantages such organization may confer for beta cell function. The development

of new tools for sorting cells based on their mRNA content (Arrigucci et al., 2017; Klemm et al., 2014; Rouhanifard et al., 2018) will facilitate deeper characterization of additional features of extreme cells such as epigenetic modifications and proteome characterization. These future studies will shed more light into the biology of this sub-population of beta cells.

### Limitations

As with traditional smFISH, our technique has lower signal to noise ratio for very short transcripts, since it requires the specific accumulation of sufficient numbers of singly labeled probes. The method currently allows simultaneous imaging of up to three genes. Notably, the protocol improvements we have performed could be combined with other technologies for smFISH that enable higher throughput through combinatorial labeling of probe libraries and multiple rounds of hybridizations (Chen et al., 2015; Lubeck et al., 2014; Moffitt and Zhuang, 2016; Shaffer et al., 2017; Shah et al., 2016). While smFISH has single-molecule resolution, discerning signal from non-specific fluorescent spots could be challenging for very lowly expressed genes. Examples of such genes of interest include some long non-coding RNA (Akerman et al., 2017) as well as disallowed beta cell genes (Pullen et al., 2017). In addition, while we presented combined detection of mRNA and protein via simultaneous immunofluorescence and smFISH (STAR Methods), the implementation of this approach strongly relies on the specificity and sensitivity of the antibodies and would require fine-tuning and optimization. The present study was confined to murine islets and will require confirmation in human islets.

## STAR★METHODS

Detailed methods are provided in the online version of this paper and include the following:

- KEY RESOURCES TABLE
- CONTACT FOR REAGENT AND RESOURCE SHARING
- EXPERIMENTAL MODEL AND SUBJECT DETAILS
  - Animal Experiments
- METHOD DETAILS
  - Islet Isolation
  - Transmission Electron Microscopy
  - Single Molecule FISH
  - Immunofluorescence
  - Imaging
- QUANTIFICATION AND STATISTICAL ANALYSIS
  - Image Analysis
  - Statistics

### SUPPLEMENTAL INFORMATION

Supplemental Information includes seven figures, one table, and one methods file and can be found with this article online at https://doi.org/10.1016/j.devcel.2018.11.001.

### ACKNOWLEDGMENTS

We thank Yuval Dor and Michael Walker for valuable comments. Electron microscopy studies were conducted at the Irving and Cherna Moskowitz Center for Nano and Bio-Nano Imaging at the Weizmann Institute of Science. We thank Hagit Shapiro and Eran Elinav for the B6.BKS(D)-Leprdb/J mice. S.I. is supported by the Henry Chanoch Krenter Institute for Biomedical Imaging and Genomics, The Leir Charitable Foundations, Richard Jakubskind Laboratory of Systems Biology, Cymerman-Jakubskind Prize, The Lord Sieff of Brimpton Memorial Fund, the I-CORE program of the Planning and Budgeting Committee and the Israel Science Foundation (grants 1902/12 and 1796/12), the Israel Science Foundation grant No. 1486/16, the EMBO Young Investigator Program and the European Research Council under the European Union's Seventh Framework Programme (FP7/2007-2013)/ERC grant agreement number 335122, the Bert L. and N. Kuggie Vallee Foundation, and the Howard Hughes Medical Institute (HHMI) international research scholar award.

### AUTHOR CONTRIBUTIONS

S.I., L.F., and M.G. conceived the study. L.F. and M.G. designed and performed most of the experiments. M.G. discovered extreme beta cells and the enrichment of transcripts from other secretory genes. M.G. characterized the apical polarization of insulin mRNA. L.F. optimized the smFISH protocol for in situ pancreatic tissue. L.F. discovered an enrichment of extreme beta cells in *db/db* mice and formulated the hypothesis of extreme beta cells being prone to basal insulin secretion. N.D. performed TEM experiments. I.G. designed the spatial analysis of extreme cells within an islet. L.F., M.G., A.E., K.B.H., and B.T. performed smFISH experiments. S.B.-M. assisted with statistical analysis. L.R. and V.K. assisted with the PDX-1-Cre;LSL-KRAS$^{G12D}$ mice. S.I. and L.F. wrote the manuscript. S.I. supervised the study. All authors discussed the results and commented on the manuscript.

### DECLARATION OF INTERESTS

The authors declare no competing interests.

Received: May 11, 2018
Revised: September 14, 2018
Accepted: October 31, 2018
Published: November 29, 2018

### SUPPORTING CITATIONS

The following reference appear in the Supplemental Information: Parikh et al., 2012.

### REFERENCES

Aguayo-Mazzucato, C., and Bonner-Weir, S. (2018). Pancreatic β cell regeneration as a possible therapy for diabetes. Cell Metab. *27*, 57–67.

Akerman, I., Tu, Z., Beucher, A., Rolando, D.M.Y., Sauty-Colace, C., Benazra, M., Nakic, N., Yang, J., Wang, H., Pasquali, L., et al. (2017). Human pancreatic β cell lncRNAs control cell-specific regulatory networks. Cell Metab. *25*, 400–411.

Arrigucci, R., Bushkin, Y., Radford, F., Lakehal, K., Vir, P., Pine, R., Martin, D., Sugarman, J., Zhao, Y., Yap, G.S., et al. (2017). FISH-Flow, a protocol for the concurrent detection of mRNA and protein in single cells using fluorescence *in situ* hybridization and flow cytometry. Nat. Protoc. *12*, 1245–1260.

Bader, E., Migliorini, A., Gegg, M., Moruzzi, N., Gerdes, J., Roscioni, S.S., Bakhti, M., Brandl, E., Irmler, M., Beckers, J., et al. (2016). Identification of proliferative and mature β-cells in the islets of Langerhans. Nature *535*, 430–434.

Bahar Halpern, K., Caspi, I., Lemze, D., Levy, M., Landen, S., Elinav, E., Ulitsky, I., and Itzkovitz, S. (2015). Nuclear retention of mRNA in mammalian tissues. Cell Rep. *13*, 2653–2662.

Baron, M., Veres, A., Wolock, S.L., Faust, A.L., Gaujoux, R., Vetere, A., Ryu, J.H., Wagner, B.K., Shen-Orr, S.S., Klein, A.M., et al. (2016). A single-cell transcriptomic map of the human and mouse pancreas reveals inter- and intra-cell population structure. Cell Syst. *3*, 346–360.e4.

Bengtsson, M., Ståhlberg, A., Rorsman, P., and Kubista, M. (2005). Gene expression profiling in single cells from the pancreatic islets of Langerhans reveals lognormal distribution of mRNA levels. Genome Res. *15*, 1388–1392.

Benitez, C.M., Goodyer, W.R., and Kim, S.K. (2012). Deconstructing pancreas developmental biology. Cold Spring Harb. Perspect. Biol. *4*, a012401.

Benninger, R.K.P., Hutchens, T., Head, W.S., McCaughey, M.J., Zhang, M., Le Marchand, S.J., Satin, L.S., and Piston, D.W. (2014). Intrinsic islet heterogeneity and gap junction coupling determine spatiotemporal $Ca^{2+}$ wave dynamics. Biophys. J. *107*, 2723–2733.

Bertram, R., Previte, J., Sherman, A., Kinard, T.A., and Satin, L.S. (2000). The phantom burster model for pancreatic beta-cells. Biophys. J. *79*, 2880–2892.

Blum, B., Hrvatin, S., Schuetz, C., Bonal, C., Rezania, A., and Melton, D.A. (2012). Functional beta-cell maturation is marked by an increased glucose threshold and by expression of urocortin 3. Nat. Biotechnol. *30*, 261–264.

Bock, T., Pakkenberg, B., and Buschard, K. (2003). Increased islet volume but unchanged islet number in ob/ob mice. Diabetes *52*, 1716–1722.

Bonner-Weir, S. (1988). Morphological evidence for pancreatic polarity of beta-cell within islets of Langerhans. Diabetes *37*, 616–621.

Buxbaum, A.R., Haimovich, G., and Singer, R.H. (2015). In the right place at the right time: visualizing and understanding mRNA localization. Nat. Rev. Mol. Cell Biol. *16*, 95–109.

Chen, K.H., Boettiger, A.N., Moffitt, J.R., Wang, S., and Zhuang, X. (2015). RNA imaging. Spatially resolved, highly multiplexed RNA profiling in single cells. Science *348*, aaa6090.

Chu, K.Y., Lin, Y., Hendel, A., Kulpa, J.E., Brownsey, R.W., and Johnson, J.D. (2010). ATP-citrate lyase reduction mediates palmitate-induced apoptosis in pancreatic beta cells. J. Biol. Chem. *285*, 32606–32615.

Cui, Y., Hu, D., Markillie, L.M., Chrisler, W.B., Gaffrey, M.J., Ansong, C., Sussel, L., and Orr, G. (2018). Fluctuation localization imaging-based fluorescence in situ hybridization (fliFISH) for accurate detection and counting of RNA copies in single cells. Nucleic Acids Res. *46*, e7.

Dalbøge, L.S., Almholt, D.L.C., Neerup, T.S.R., Vassiliadis, E., Vrang, N., Pedersen, L., Fosgerau, K., and Jelsing, J. (2013). Characterisation of age-dependent beta cell dynamics in the male db/db mice. PLoS One *8*, e82813.

Dor, Y., Brown, J., Martinez, O.I., and Melton, D.A. (2004). Adult pancreatic beta-cells are formed by self-duplication rather than stem-cell differentiation. Nature *429*, 41–46.

Dorrell, C., Schug, J., Canaday, P.S., Russ, H.A., Tarlow, B.D., Grompe, M.T., Horton, T., Hebrok, M., Streeter, P.R., Kaestner, K.H., et al. (2016). Human islets contain four distinct subtypes of β cells. Nat. Commun. *7*, 11756.

Eldar, A., and Elowitz, M.B. (2010). Functional roles for noise in genetic circuits. Nature *467*, 167–173.

Elowitz, M.B., Levine, A.J., Siggia, E.D., and Swain, P.S. (2002). Stochastic gene expression in a single cell. Science *297*, 1183–1186.

Ferreira, R.M.M., Sancho, R., Messal, H.A., Nye, E., Spencer-Dene, B., Stone, R.K., Stamp, G., Rosewell, I., Quaglia, A., and Behrens, A. (2017). Duct- and acinar-derived pancreatic ductal adenocarcinomas show distinct tumor progression and marker expression. Cell Rep. *21*, 966–978.

Gan, W.J., Zavortink, M., Ludick, C., Templin, R., Webb, R., Webb, R., Ma, W., Poronnik, P., Parton, R.G., Gaisano, H.Y., et al. (2017). Cell polarity defines three distinct domains in pancreatic β-cells. J. Cell Sci. *130*, 143–151.

Gao, T., McKenna, B., Li, C., Reichert, M., Nguyen, J., Singh, T., Yang, C., Pannikar, A., Doliba, N., Zhang, T., et al. (2014). Pdx1 maintains β cell identity and function by repressing an α cell program. Cell Metab. *19*, 259–271.

Gembal, M., Gilon, P., and Henquin, J.C. (1992). Evidence that glucose can control insulin release independently from its action on ATP-sensitive K+ channels in mouse B cells. J. Clin. Invest. *89*, 1288–1295.

Geron, E., Boura-Halfon, S., Schejter, E.D., and Shilo, B.Z. (2015). The edges of pancreatic islet β cells constitute adhesive and signaling microdomains. Cell Rep. *10*, 317–325.

Granot, Z., Swisa, A., Magenheim, J., Stolovich-Rain, M., Fujimoto, W., Manduchi, E., Miki, T., Lennerz, J.K., Stoeckert, C.J., Meyuhas, O., et al. (2009). LKB1 regulates pancreatic β cell size, polarity, and function. Cell Metab. *10*, 296–308.

Gutierrez, G.D., Gromada, J., and Sussel, L. (2017). Heterogeneity of the pancreatic beta cell. Front. Genet. *8*, 22.

Haataja, L., Snapp, E., Wright, J., Liu, M., Hardy, A.B., Wheeler, M.B., Markwardt, M.L., Rizzo, M., and Arvan, P. (2013). Proinsulin intermolecular interactions during secretory trafficking in pancreatic β cells. J. Biol. Chem. *288*, 1896–1906.

Halpern, K.B., Shenhav, R., Matcovitch-Natan, O., Tóth, B., Lemze, D., Golan, M., Massasa, E.E., Baydatch, S., Landen, S., Moor, A.E., et al. (2017). Single-cell spatial reconstruction reveals global division of labour in the mammalian liver. Nature *542*, 352–356.

Henquin, J.C., Nenquin, M., Stiernet, P., and Ahren, B. (2006). In vivo and in vitro glucose-induced biphasic insulin secretion in the mouse: pattern and role of cytoplasmic Ca2+ and amplification signals in β-cells. Diabetes *55*, 441–451.

Hingorani, S.R., Petricoin, E.F., Maitra, A., Rajapakse, V., King, C., Jacobetz, M.A., Ross, S., Conrads, T.P., Veenstra, T.D., Hitt, B.A., et al. (2003). Preinvasive and invasive ductal pancreatic cancer and its early detection in the mouse. Cancer Cell *4*, 437–450.

Itzkovitz, S., and van Oudenaarden, A. (2011). Validating transcripts with probes and imaging technology. Nat. Methods *8*, S12–S19.

Itzkovitz, S., Lyubimova, A., Blat, I.C., Maynard, M., van Es, J., Lees, J., Jacks, T., Clevers, H., and van Oudenaarden, A. (2011). Single-molecule transcript counting of stem-cell markers in the mouse intestine. Nat. Cell Biol. *14*, 106–114.

Johnston, N.R., Mitchell, R.K., Haythorne, E., Pessoa, M.P., Semplici, F., Ferrer, J., Piemonti, L., Marchetti, P., Bugliani, M., Bosco, D., et al. (2016). Beta cell hubs dictate pancreatic islet responses to glucose. Cell Metab. *24*, 389–401.

Jørgensen, M.C., Ahnfelt-Rønne, J., Hald, J., Madsen, O.D., Serup, P., and Hecksher-Sørensen, J. (2007). An illustrated review of early pancreas development in the mouse. Endocr. Rev. *28*, 685–705.

Kiekens, R., In 't Veld, P., Mahler, T., Schuit, F., Van De Winkel, M., and Pipeleers, D. (1992). Differences in glucose recognition by individual rat pancreatic B cells are associated with intercellular differences in glucose-induced biosynthetic activity. J. Clin. Invest. *89*, 117–125.

Kim, Y.H., Larsen, H.L., Rué, P., Lemaire, L.A., Ferrer, J., and Grapin-Botton, A. (2015). Cell cycle–dependent differentiation dynamics balances growth and endocrine differentiation in the pancreas. PLoS Biol. *13*, e1002111.

Klemm, S., Semrau, S., Wiebrands, K., Mooijman, D., Faddah, D.A., Jaenisch, R., and van Oudenaarden, A. (2014). Transcriptional profiling of cells sorted by RNA abundance. Nat. Methods *11*, 549–551.

Klochendler, A., Caspi, I., Corem, N., Moran, M., Friedlich, O., Elgavish, S., Nevo, Y., Helman, A., Glaser, B., Eden, A., et al. (2016). The genetic program of pancreatic beta-cell replication in vivo. Diabetes *65*, 2081–2093.

Li, J., Klughammer, J., Farlik, M., Penz, T., Spittler, A., Barbieux, C., Berishvili, E., Bock, C., and Kubicek, S. (2016). Single-cell transcriptomes reveal characteristic features of human pancreatic islet cell types. EMBO Rep. *17*, 178–187.

Little, S.C., Tikhonov, M., and Gregor, T. (2013). Precise developmental gene expression arises from globally stochastic transcriptional activity. Cell *154*, 789–800.

Lubeck, E., Coskun, A.F., Zhiyentayev, T., Ahmad, M., and Cai, L. (2014). Single-cell in situ RNA profiling by sequential hybridization. Nat. Methods *11*, 360–361.

Lyubimova, A., Itzkovitz, S., Junker, J.P., Fan, Z.P., Wu, X., and van Oudenaarden, A. (2013). Single-molecule mRNA detection and counting in mammalian tissue. Nat. Protoc. *8*, 1743–1758.

Martin, K.C., and Ephrussi, A. (2009). mRNA localization: gene expression in the spatial dimension. Cell *136*, 719–730.

Mastronarde, D.N. (2005). Automated electron microscope tomography using robust prediction of specimen movements. J. Struct. Biol. *152*, 36–51.

McCulloch, L.J., van de Bunt, M., Braun, M., Frayn, K.N., Clark, A., and Gloyn, A.L. (2011). GLUT2 (SLC2A2) is not the principal glucose transporter in human pancreatic beta cells: implications for understanding genetic association signals at this locus. Mol. Genet. Metab. *104*, 648–653.

van der Meulen, T., Mawla, A.M., DiGruccio, M.R., Adams, M.W., Nies, V., Dólleman, S., Liu, S., Ackermann, A.M., Cáceres, E., Hunter, A.E., et al.

(2017). Virgin beta cells persist throughout life at a neogenic niche within pancreatic islets. Cell Metab. *25*, 911–926.e6.

Michael, D.J., Ritzel, R.A., Haataja, L., and Chow, R.H. (2006). Pancreatic β-cells secrete insulin in fast- and slow-release forms. Diabetes *55*, 600–607.

Moffitt, J.R., and Zhuang, X. (2016). RNA imaging with multiplexed error-robust fluorescence in situ hybridization (MERFISH). Methods Enzymol. *572*, 1–49.

Moor, A.E., Golan, M., Massasa, E.E., Lemze, D., Weizman, T., Shenhav, R., Baydatch, S., Mizrahi, O., Winkler, R., Golani, O., et al. (2017). Global mRNA polarization regulates translation efficiency in the intestinal epithelium. Science *357*, 1299–1303.

Muraro, M.J., Dharmadhikari, G., Grün, D., Groen, N., Dielen, T., Jansen, E., van Gurp, L., Engelse, M.A., Carlotti, F., de Koning, E.J.P., et al. (2016). A single-cell transcriptome atlas of the human pancreas. Cell Syst. *3*, 385–394.e3.

Nir, T., Melton, D.A., and Dor, Y. (2007). Recovery from diabetes in mice by beta cell regeneration. J. Clin. Invest. *117*, 2553–2561.

Orci, L., Thorens, B., Ravazzola, M., and Lodish, H.F. (1989). Localization of the pancreatic beta cell glucose transporter to specific plasma membrane domains. Science *245*, 295–297.

Pagliuca, F.W., and Melton, D.A. (2013). How to make a functional β-cell. Development *140*, 2472–2483.

Parikh, A., Stephan, A.F., and Tzanakakis, E.S. (2012). Regenerating proteins and their expression, regulation and signaling. Biomol. Concepts *3*, 57–70.

Pfeifer, M.A., Halter, J.B., and Porte, D. (1981). Insulin secretion in diabetes mellitus. Am. J. Med. *70*, 579–588.

Porat, S., Weinberg-Corem, N., Tornovsky-Babaey, S., Schyr-Ben-Haroush, R., Hija, A., Stolovich-Rain, M., Dadon, D., Granot, Z., Ben-Hur, V., White, P., et al. (2011). Control of pancreatic β cell regeneration by glucose metabolism. Cell Metab. *13*, 440–449.

Pullen, T.J., Huising, M.O., and Rutter, G.A. (2017). Analysis of purified pancreatic islet beta and alpha cell transcriptomes reveals 11β-hydroxysteroid dehydrogenase (Hsd11b1) as a novel disallowed gene. Front. Genet. *8*, 41.

Raj, A., and van Oudenaarden, A. (2008). Nature, nurture, or chance: stochastic gene expression and its consequences. Cell *135*, 216–226.

Raj, A., van den Bogaard, P., Rifkin, S.A., van Oudenaarden, A., and Tyagi, S. (2008). Imaging individual mRNA molecules using multiple singly labeled probes. Nat. Methods *5*, 877–879.

Regev, A., Teichmann, S.A., Lander, E.S., Amit, I., Benoist, C., Birney, E., Bodenmiller, B., Campbell, P., Carninci, P., Clatworthy, M., et al. (2017). The human cell atlas. Elife *6*, https://doi.org/10.7554/eLife.27041.

Rhodes, C.J. (2005). Type 2 diabetes-a matter of β-cell life and death? Science *307*, 380–384.

Roscioni, S.S., Migliorini, A., Gegg, M., and Lickert, H. (2016). Impact of islet architecture on β-cell heterogeneity, plasticity and function. Nat. Rev. Endocrinol. *12*, 695–709.

Rouhanifard, S.H., Mellis, I.A., Dunagin, M., Bayatpour, S., Jiang, C.L., Dardani, I., Symmons, O., Emert, B., Torre, E., Cote, A., et al. (2018). ClampFISH detects individual nucleic acid molecules using click chemistry-based amplification. Nat. Biotechnol. Nov 12. https://doi.org/10.1038/nbt.4286.

Salomon, D., and Meda, P. (1986). Heterogeneity and contact-dependent regulation of hormone secretion by individual B cells. Exp. Cell Res. *162*, 507–520.

Sander, M., and German, M.S. (1997). The β cell transcription factors and development of the pancreas. J. Mol. Med. *75*, 327–340.

Schindelin, J., Arganda-Carreras, I., Frise, E., Kaynig, V., Longair, M., Pietzsch, T., Preibisch, S., Rueden, C., Saalfeld, S., Schmid, B., et al. (2012). Fiji: an open-source platform for biological-image analysis. Nat. Methods *9*, 676–682.

Schwanhäusser, B., Busse, D., Li, N., Dittmar, G., Schuchhardt, J., Wolf, J., Chen, W., and Selbach, M. (2011). Global quantification of mammalian gene expression control. Nature *473*, 337–342.

Segerstolpe, Å., Palasantza, A., Eliasson, P., Andersson, E.M., Andréasson, A.C., Sun, X., Picelli, S., Sabirsh, A., Clausen, M., Bjursell, M.K., et al. (2016). Single-cell transcriptome profiling of human pancreatic islets in health and type 2 diabetes. Cell Metab. *24*, 593–607.

Shaffer, S.M., Dunagin, M.C., Torborg, S.R., Torre, E.A., Emert, B., Krepler, C., Beqiri, M., Sproesser, K., Brafford, P.A., Xiao, M., et al. (2017). Rare cell variability and drug-induced reprogramming as a mode of cancer drug resistance. Nature *546*, 431–435.

Shah, S., Lubeck, E., Zhou, W., and Cai, L. (2016). In situ transcription profiling of single cells reveals spatial organization of cells in the mouse hippocampus. Neuron *92*, 342–357.

Singh, S.P., Janjuha, S., Hartmann, T., Kayisoglu, Ö., Konantz, J., Birke, S., Murawala, P., Alfar, E.A., Murata, K., Eugster, A., et al. (2017). Different developmental histories of beta-cells generate functional and proliferative heterogeneity during islet growth. Nat. Commun. *8*, 664.

Szot, G.L., Koudria, P., and Bluestone, J.A. (2007). Murine pancreatic islet isolation. J. Vis. Exp. 255, https://doi.org/10.3791/255.

Takahashi, N., Kishimoto, T., Nemoto, T., Kadowaki, T., and Kasai, H. (2002). Fusion pore dynamics and insulin granule exocytosis in the pancreatic islet. Science *297*, 1349–1352.

Thorens, B., and Roduit, R. (1994). Regulated expression of GLUT2 in diabetes studied in transplanted pancreatic beta cells. Biochem. Soc. Trans. *22*, 684–687.

Unger, R.H., and Orci, L. (2010). Paracrinology of islets and the paracrinopathy of diabetes. Proc. Natl. Acad. Sci. USA *107*, 16009–16012.

Van De Winkel, M., and Pipeleers, D. (1983). Autofluorescence-activated cell sorting of pancreatic islet cells: purification of insulin-containing B-cells according to glucose-induced changes in cellular redox state. Biochem. Biophys. Res. Commun. *114*, 835–842.

Wang, Y.J., Schug, J., Won, K.J., Liu, C., Naji, A., Avrahami, D., Golson, M.L., and Kaestner, K.H. (2016). Single-cell transcriptomics of the human endocrine pancreas. Diabetes *65*, 3028–3038.

Weir, G.C., and Bonner-Weir, S. (1990). Islets of Langerhans: the puzzle of intraislet interactions and their relevance to diabetes. J. Clin. Invest. *85*, 983–987.

Welsh, M., Nielsen, D.A., MacKrell, A.J., and Steiner, D.F. (1985). Control of insulin gene expression in pancreatic beta-cells and in an insulin-producing cell line, RIN-5F cells. II. Regulation of insulin mRNA stability. J. Biol. Chem. *260*, 13590–13594.

Wentworth, B.M., Schaefer, I.M., Villa-Komaroff, L., and Chirgwin, J.M. (1986). Characterization of the two nonallelic genes encoding mouse preproinsulin. J. Mol. Evol. *23*, 305–312.

Yachida, S., Jones, S., Bozic, I., Antal, T., Leary, R., Fu, B., Kamiyama, M., Hruban, R.H., Eshleman, J.R., Nowak, M.A., et al. (2010). Distant metastasis occurs late during the genetic evolution of pancreatic cancer. Nature *467*, 1114–1117.

Zeng, C., Mulas, F., Sui, Y., Guan, T., Miller, N., Tan, Y., Liu, F., Jin, W., Carrano, A.C., Huising, M.O., et al. (2017). Pseudotemporal ordering of single cells reveals metabolic control of postnatal β cell proliferation. Cell Metab. *25*, 1160–1175.e11.

# STAR★METHODS

## KEY RESOURCES TABLE

| REAGENT or RESOURCE | SOURCE | IDENTIFIER |
|---|---|---|
| Antibodies | | |
| Guinea pig polyclonal anti-Insulin | Dako | Cat# A0564; RRID: AB_10013624 |
| Mouse monoclonal anti-Proinsulin | Developmental Studies Hybridoma Bank, DSHB | Cat# GS-9A8-c; RRID: AB_532383 |
| Goat Anti-Guinea pig IgG H&L (FITC) | Abcam | Cat# ab6904; RRID: AB_955277 |
| Goat anti-Mouse IgG (H+L) Cross-Adsorbed Secondary Antibody, Alexa Fluor 594 | Thermo Fisher | Cat# A11005; RRID: AB_2534073 |
| Biological Samples | | |
| BSA, nuclease-free, 50 mg $ml^{-1}$ | Ambion | Cat# AM2616 |
| Albumin Bovine, Fraction V | MP | Cat# 160069 |
| Normal Horse Serum Blocking Solution | Vector laboratories | Cat# S-2000 |
| Chemicals, Peptides, and Recombinant Proteins | | |
| Alexa Fluor™ 488 Phalloidin | Thermo Fisher | Cat# A12379 |
| Rhodamine Phalloidin | Thermo Fisher | Cat# R415 |
| 6-Carboxytetramethylrhodamine succinimidyl ester (TMR) | Molcular probes | Cat# C6123 |
| Cy5 succinimidyl ester | GE Healthcare | Cat# PA25001 |
| Alexa Fluor 594 carboxylic acid succinimidyl ester | Thermo Fisher | Cat# A37572 |
| Formaldehyde, 37% (w/v) | J.T. Baker | Cat# JT2106 |
| Formamide, deionized, nuclease-free | Ambion | Cat# AM9342 |
| O.C.T. Compound Cryostat Embedding Medium | Scigen | Cat# 4586 |
| DAPI | Sigma-Aldrich | Cat# D9542 |
| Water UltraPure Dnase/RNase-free Molecular Biology | Bio-Lab | Cat# 23217723 |
| PBS, pH 7.4, RNase-free, 10× | Ambion | Cat# AM9625 |
| ProLong™ Gold Antifade Mountant | Molecular Probes | Cat# P36934 |
| RPMI 1640 Medium, no glutamine | Biological Industries | Cat# 01-101-1A |
| Collagenase P | Sigma-Aldrich | Cat# 11213865001 |
| Histopaque®-1119 | Sigma-Aldrich | Cat# 1119 |
| Histopaque®-1077 | Sigma-Aldrich | Cat# 1077 |
| Caerulein | Sigma-Aldrich | Cat# C9026 |
| Diazoxide | Sigma-Aldrich | Cat# D9035 |
| 16% Paraformaldehyde (formaldehyde) aqueous solution | Electron Microscopy Sciences | Cat# 50-980-487 |
| Aqueous Glutaraldehyde 8% | Electron Microscopy Sciences | Cat# 50-262-18 |
| Sucrose | J.T.Baker | Cat# 4072 |
| Dimethylarsinic acid sodium salt trihydrate | Merck | Cat# 8.20670.0250 |
| Calcium Chloride dihydrate | Sigma-Aldrich | Cat# 223506-500G |
| Osmium Tetroxide, 4% Aqueous Solution | Electron Microscopy Sciences | Cat# 19150 |
| Agar 100 resin kit | Agar scientific | Cat# AGR1031 |
| 4% Uranyl Acetate Solution | EMS | Cat# C993L52, Mfr. No. 22400-4 |
| Sodium Citrate | Avantor | Cat# 0754-12 |
| Lead (II) Nitrate | Merck | Cat# 1.07398.0100 |
| Potassium dichromate | Merck | Cat# 104865 |
| Potassium hexacyonaferrate | Merck | Cat# 104982 |

(*Continued on next page*)

*Continued*

| REAGENT or RESOURCE | SOURCE | IDENTIFIER |
|---|---|---|
| Experimental Models: Organisms/Strains | | |
| C57BL/6 inbred mice | Envigo | Strain: C57BL/6JOlaHsd |
| B6.BKS(D)-Leprdb/J mice on C57BL/6J genetic background | The Jackson Laboratory | Cat# JAX:000697; RRID: IMSR_JAX:000697 |
| B6.FVB-Tg(Pdx1-cre)6Tuv/J | The Jackson Laboratory | Cat# JAX:014647; RRID: IMSR_JAX:014647 |
| B6.129S4-Kras$^{tm4Tyj}$/J | The Jackson Laboratory | Cat# JAX:008179; RRID: IMSR_JAX:008179 |
| Oligonucleotides | | |
| smFISH probes, see Table S1 | This paper | N/A |
| Software and Algorithms | | |
| Stellaris FISH Probe Designer | Biosearch Technologies | http://singlemoleculefish.com/ |
| R and RStudio v3.4.1 | R Consortium | https://www.rstudio.com/ |
| MATLAB R2016b | MathWorks® | https://www.mathworks.com/ |
| ImageM | Lyubimova et al. (2013) | N/A |
| ImageJ 1.51h | Schindelin et al. (2012) | https://imagej.nih.gov/ij/ |
| MetaMorph software | Molecular Devices, Downington, PA | https://www.biocompare.com/19333-Image-Analysis-Software-Image-Processing-Software/78845-MetaMorphreg-Microscopy-Automation-Image-Analysis-Software/ |
| SerialEM | Mastronarde (2005) | http://bio3d.colorado.edu/SerialEM/ |

## CONTACT FOR REAGENT AND RESOURCE SHARING

Further information and requests for resources and reagents should be directed to and will be fulfilled by the Lead Contact, Shalev Itzkovitz (shalev.itzkovitz@weizmann.ac.il).

## EXPERIMENTAL MODEL AND SUBJECT DETAILS

### Animal Experiments

All animal experiments were performed with institutional guidelines and approved by the institutional Animal Care and Use Committee of the Weizmann Institute of Science. All mice were housed in a specific pathogen-free facility in individually ventilated cages on a strict 12-h light–dark cycle. C57BL/6 were purchased from Envigo and allowed to acclimatize to the animal facility environment for at least 3 days before being used for experimentation. C57BL/6 male mice aged 8-9 weeks were fasted for 8-12 h with free access to water and sacrificed between ZT3-ZT5. Homozygous B6.BKS(D)-Leprdb/J mice on C57BL/6J genetic background (*db/db*) and age-matched controls were bred in the in the institutional animal facility and previously obtained from Jackson Laboratory. In Figure 6, male *db/db* mice and control C57BL/6J aged 14-15 weeks with *ad libitum* access to water and standard laboratory diet were used. In Figure S4, a female *db/db* mouse aged 32 weeks was fasted for 12 h. Body weight and blood glucose level for *db/db* and control mice are shown in Figures S6B–S6G. PDX1-Cre mice and LSL-KrasG12D mice were obtained from Jackson Laboratories (Bar Harbor). PDX-1-Cre;LSL-KRAS$^{G12D}$ mice were bred in the institutional animal facility. The presence of floxed LSL-krasG12D and PDX1-Cre alleles was verified by PCR. For induction of acute pancreatitis PDX-1-Cre;LSL-KRAS$^{G12D}$ mice were subjected to a series of seven hourly intra- peritoneal injections of Caerulein (Sigma, C9026. 50 μg/kg of body weight). In Figures S7C–S7E, a female mouse that had developed pancreatic cancer was sacrificed 3 weeks after injection at the age of 3 months. All mice were sacrificed by cervical dislocation. For smFISH, pancreas tissues were collected and fixed in RNase-free 4% formaldehyde for 3 h; incubated overnight with 30% sucrose in 4% formaldehyde and then embedded in OCT. 5 μm cryosections were used for hybridization and immunofluorescence. Each smFISH result was based on at least 2 mice. No statistical methods were used to predetermine sample size.

## METHOD DETAILS

### Islet Isolation

Islets were isolated using collagenase P digestion as previously described (Szot et al., 2007). In brief, mice were sacrificed with cervical dislocation. The pancreas was inflated through the bile duct with 3 ml 0.7 mg/ml Collagenase P (Roche, 1.8 U/mg lyophilizate) in RPMI 1640 solution (Biological Industries, without L-glutamine). The inflated pancreas was incubated at 37°C for 7 min and then placed on ice for not more than 1 h. The tissue was washed and dissociated further by adding 10 ml RPMI medium and shaking vigorously. The tissue was spun down at 1000 rpm for 1 minute. The supernatant was discarded and the washing step repeated twice. The

supernatant was removed and the tissue was re-suspended in 4 ml Histopaque (Sigma 11191) in a 15 ml falcon tube. To the same tube, 4 ml of Histopaque (Sigma 10771) was added dropwise followed by 3 ml of RPMI medium. Centrifugation was set to 2500 rpm at 4°C without brakes and acceleration for 20 min to separate pancreatic islets from the exocrine tissue. Islets were picked with a Pasteur pipette and washed twice with 10 ml RPMI 1640 complete medium (11mM glucose, 10% FBS, 1% penicilin/streptomycin, and 1% L-glutamine). Islets were handpicked under the binocular.

### Transmission Electron Microscopy

Following isolation, pancreatic islets were immediately fixed with 3% paraformaldehyde (Electron Micrsocopy Sciences, EMS), 2% glutaraldehyde (EMS), 3% sucrose (J.T. Baker) in 0.1 M cacodylate buffer containing 5 mM $CaCl_2$ (pH 7.4), postfixed in 1% osmium tetroxide (EMS) supplemented with 0.5% potassium hexacyanoferrate tryhidrate (Merck) and potasssium dichromate (Merck) in 0.1 M cacodylate for 1 h, stained with 2% uranyl acetate (EMS) in double distilled water for 1 h, dehydrated in graded ethanol solutions and embedded in epoxy resin (Agar scientific Ltd., Stansted, UK). Ultrathin sections (70-90 nm) obtained with an Ultracut UCT microtome (Leica) were stained with lead citrate and then examined using a FEI Tecnai SPIRIT (FEI, Eidhoven, Netherlands) transmission electron microscope operated at 120 kV. Images were recorded either with a bottom mounted 2k X 2k Eagle CCD camera (FEI, Eindhoven; Figure 5G left panel) or a MegaView III side-mounted Olympus TEM CCD camera (Olympus Ireland, Dublin; Figure 5G right panel; Figures S5B and S5C). Figure S5A, images were recorded using a Philips CM-12 transmission electron microscope equipped with a Gatan OneView camera. Serial sections were stitched with the Software SerialEM (Mastronarde, 2005). To quantify the fraction of putative extreme cells in the TEM images we included all beta cells with an apparent nucleus in the sectioned slice (224 cells). Extreme cells were identified as cells with an expanded ER close to the cell border and low insulin granule counts.

### Single Molecule FISH

The construction of the probe library, hybridization procedure and imaging conditions were previously described (Itzkovitz et al., 2011; Lyubimova et al., 2013; Raj et al., 2008). A detailed description of the protocol is given in the Supplementary protocol file (Methods S1). In brief, probe libraries were designed using the Stellaris FISH Probe Designer (Biosearch Technologies, Inc., Petaluma, CA). Libraries consisted of 17-96 probes each of length 20 bps, complementary to the coding sequence of each gene (Table S1). As a modification of the standard tissue smFISH protocol (Lyubimova et al., 2013), formamide concentration of the washing and hybridization buffers were increased to 30%. Notably, the washing buffer has to be prepared fresh. In addition, an elongated incubation of at least 3 hours with the washing buffer was applied before hybridizing with the probe libraries. smFISH probe libraries were coupled to Cy5 (GE Healthcare, PA25001), Alexa594 (Thermo Fisher, A37572) and TMR (Molecular Probes, C6123). Nuclei were stained with Dapi (Sigma-Aldrich, D9542). To detect cell borders, alexa fluor 488 conjugated phalloidin (Thermo Fisher, A12379) or rhodamine conjugated phalloidin (Thermo Fisher, R415), was added to the GLOX buffer wash for 15 minutes. Slides were mounted using ProLong Gold (Molecular Probes, P36934). Beta cells were detected according to their insulin smFISH or antibody signal.

### Immunofluorescence

To combine smFISH and immunofluorescence, OCT embedded tissues were sectioned (5 μm), fixed with 4% Formaldehyde, and permeabilized with 70% ethanol for 2 hours. Antigen retrieval required for Proinsulin was carried out by boiling citrate buffer (pH 6) for 10 minutes and slowly cooling down to room temperature thereafter. Sections were washed in RNase-free PBST (0.1% Tween) before and after proceeding with the smFISH protocol (Methods S1; steps 15–24). Following the hybridization with the probe libraries and washing with 30% formamide wash buffer, the sections were blocked and incubated for 1h at room temperature with guinea pig anti-Insulin antibody 1:1000 (Dako, A0564) and mouse anti-proinsulin 1:50 (DSHB, GS-9A8-c). Detection was performed with the secondary antibodies goat anti-guinea pig FITC 1:200 (Abcam, ab6904), goat anti-mouse Alexa Fluor 594 1:200 (Thermo Fisher, A11005) for 1 hour at room temperature.

### Imaging

smFISH imaging was performed on a Nikon-Ti-E inverted fluorescence microscope equipped with a 100×oil-immersion objective and a Photometrics Pixis 1024 CCD camera using MetaMorph software (Molecular Devices, Downington, PA) as previously reported (Itzkovitz et al., 2011). The image-plane pixel dimension was 0.13 μm. Quantification was performed on stacks of five optical sections with *Z* spacing of 0.3 μm, in which not more than a single cell was observed.

## QUANTIFICATION AND STATISTICAL ANALYSIS

### Image Analysis

ImageM, a custom Matlab program (Lyubimova et al., 2013), was used to compute single-cell mRNA concentrations by segmenting each cell manually according to the cell borders and the nucleus. The selection of beta cells was verified by insulin smFISH or antibody staining.

The size of the nucleus was detected automatically by the program according to the DAPI signal. For each cell, the cytoplasmic mRNA and protein concentration was calculated as the mean background-subtracted intensity. For each channel, the background signal was defined by first calculating the median intensity of all nuclear voxels for each cell and z-stack and then by calculating the

median of the lower 50 percentile nuclear intensities of all segmented cells. For Ins2, Ins1, Iapp, Chga, Pcsk2, and Rn28s transcript concentrations of each beta cell were measured by cytoplasmic cell intensity. To this end, for each cell we computed the average background-subtracted voxel intensity over all cytoplasmic voxels. Extreme beta cells were defined as cells for which insulin expression exceeded 2-fold the median insulin expression within the containing islet. For other genes with lower transcript numbers and single dot resolution the transcript concentration was calculated by the number of all cellular dots per cell volume. For Abcc8 only cytoplasmic transcripts were considered, since it exhibited elevated nuclear retention of mRNA (Bahar Halpern et al., 2015). The concentration of proinsulin was calculated by the summed dot intensity for each cell. For all methods of quantification, we normalized the concentrations by the median transcript concentration of the corresponding islet. Thus, expression was computed in units of multiple of the median (MoM) cell intensity.

Line profiles for single cells (Figure 5) were generated using ImageJ and set from basal to apical. We used the ImageJ plugin plot profile to calculate the line profile for every channel (Moor et al., 2017; Schindelin et al., 2012). Each line profile was normalized to the minimum and maximum intensity. For extreme beta cells, the polar domains and the non-polar cytoplasmic domains (Figures 5E and 5F) were manually segmented with ImageJ according to insulin mRNA intensity. For each domain, single transcripts were detected automatically with ImageM. The transcript concentrations were calculated as the transcript number per volume. The expression of rRNA Rn28s was measured by the mean background-subtracted intensity for each domain. The background was estimated by the 5 percentile image intensity. Images were visualized and processed using ImageJ 1.51h (Schindelin et al., 2012) and Adobe Illustrator CC2018. In Figures S7C–S7E, images were processed using ImageJ plugins by first subtracting the background (rolling ball radius 1), smoothing, multiplying by 5, and adding the amplified dot signal to the original image. Figures 1A and S7A were processed with a Laplacian of Gaussian filter (Itzkovitz et al., 2011). Figures 1A and S6A were stitched with ImageJ.

## Statistics

P-values for comparison of expression were obtained by Wilcoxon rank-sum tests on extreme and non-extreme beta cells unless otherwise stated. Statistical analysis and data visualization were performed with MATLAB R2016b and RStudio v3.4.1. Boxplots were created with MATLAB, PlotStyle traditional. Box plot elements: center line, median; box limits, first to third quartile (Q1 to Q3); whiskers, extend to the most extreme data point within 1.5× the interquartile range (IQR) from the box; circles, data points; red crosses indicate outliers. The distribution of cellular insulin mRNA was fitted to a normal and a log-normal distribution (Figure S2). The fitted sample data was displayed as a Quantile-Quantile plot, QQ plot, versus the theoretical data of a Standard Normal distribution.

To determine whether extreme beta cells were spatially clustered (Figure S3B), we fully segmented and analyzed 31 islets from 7 mice. We created a graph for each islet, in which cells were nodes and cells separated by less than 4 μm were connected by an edge. We calculated the mean shortest path distance along the graph among all pairs of cells within the top 10% expression range of insulin. To obtain a p-value we randomly shuffled the expression values among islet cells and recalculated the mean graph distance over 1,000 iterations. We used the real and randomized mean graph distances among top 10% cells to calculate a Z-score and used the normal distribution to obtain p-values. We used Fisher's method to combine p-values for all islets. For each islet, we removed cells with insulin levels below the 10 percentile value when reshuffling, to avoid including rare segmented non-beta cells. To assess the radial preference of extreme cells we computed the distance of each extreme cell to the islet periphery, defined as the convex hull of all islet-segmented cells and normalized by the radius of the islet, defined as half of the maximal inter-cellular distance.